SEMARAK ILMU PUBLISHING

Journal of Advanced Research in Applied Mechanics

Journal homepage:
https://semarakilmu.com.my/journals/index.php/appl_mech/index
ISSN: 2289-7895

Stress Intensity Factors for Thermoelectric Bonded Materials Weakened by an Inclined Crack

Muhammad Haziq Iqmal Mohd Nordin[1], Khairum Hamzah[1,4,*], Nik Mohd Asri Nik Long[2], Najiyah Safwa Khashi'ie[3,4], Iskandar Waini[1,4], Nurul Amira Zainal[3,4] and Sayed Kushairi Sayed Nordin[3,4]

[1] Fakulti Teknologi dan Kejuruteraan Industri dan Pembuatan, Universiti Teknikal Malaysia Melaka, Hang Tuah Jaya, 76100 Durian Tunggal, Melaka, Malaysia
[2] Department of Mathematics and Statistics, Faculty of Science, Universiti Putra Malaysia, 43400 Serdang, Selangor, Malaysia
[3] Fakulti Teknologi dan Kejuruteraan Mekanikal, Universiti Teknikal Malaysia Melaka, Hang Tuah Jaya, 76100 Durian Tunggal, Melaka, Malaysia
[4] Forecasting and Engineering Technology Analysis (FETA) Research Group, Universiti Teknikal Malaysia Melaka, 76100 Durian Tunggal, Melaka, Malaysia

ARTICLE INFO

Article history:
Received 7 September 2023
Received in revised form 9 October 2023
Accepted 26 November 2023
Available online 3 January 2024

Keywords:
Thermoelectric; bonded materials; inclined crack; hypersingular integral equations; stress intensity factors

ABSTRACT

Thermoelectric Bonded Materials (TEBM) weakened by an Inclined Crack Problems (ICP) subjected to remote stress was presented in this study. The problems are addressed by employing the Modified Complex Variable Function (MCVF) method, which incorporates the Continuity Conditions (CC) for the Resultant Electric Force (REF) and Displacement Electric Function (DEF) to formulate the Hypersingular Integral Equations (HSIEs) associated with these problems. By applying the curved length coordinate method, the unknown functions of Crack Opening Displacement (COD), Electric Current Density (ECD), and Energy Flux Load (EFL) are mapped onto the square root singularity function. The resulting equations are then numerically solved using appropriate quadrature formulas, with the traction along the crack utilized as the right-hand term. The obtained COD, ECD and EFL functions is then used to compute the dimensionless Stress Intensity Factors (SIFs) in order to determine the stability behavior of TEBM weakened by an ICP. The numerical results provided demonstrate the dimensionless SIFs at the crack tips. These results exhibit excellent agreement with previous studies conducted on the subject. Additionally, it is observed that the dimensionless SIFs at the crack tips are influenced by factors such as the ratio of Elastic Constants (ECR), the geometry of the cracks, and the coefficients associated with the Electric Current Density (ECD).

1. Introduction

Materials stability and safety are critical issues in engineering structures, and the presence of cracks may jeopardize the material's strength. If the materials exposed to a temperature difference, then this material generates an electrical voltage. Cracks in thermoelectric (TE) materials can have a significant impact on their performance and durability, so it is critical to carefully control the

* *Corresponding author.*
E-mail address: khairum@utem.edu.my

https://doi.org/10.37934/aram.113.1.5262

manufacturing process and minimize crack formation in order to optimize their TE properties. Previous works utilized a variety of methods to investigate crack problems in TE materials subjected to remote-stress [1-5].

Investigating the transient response of an inner finite-size crack located arbitrarily within TE materials, the study employed singularity integral equations based on the Fourier and Laplace transforms [1]. The analysis revealed that when the crack is positioned centrally in the vertical-direction, the field concentrations at the crack tip become more prominent. Additionally, the study found that the electrical permeability of the crack has a negligible impact on the efficiency of energy conversion. The Complex Variable Function (CVF) method and conformal mapping theory were applied to investigate a two-dimensional problem involving a circular hole with two unequal cracks in infinite TE materials under uniform Electric Current Density (ECD) and Energy Flux Load (EFL) [2]. The study revealed that the behavior of the TE field and Stress Intensity Factors (SIFs) is dependent on the radius of the circular-hole and the lengths of the cracks. The CVF method was use to investigate the dimensionless SIFs for the two-dimensional problem of a crack in TE materials [3]. At the crack tip, the ECD, EFL, and stress display the conventional square-root singularity behavior.

Moreover, the SIFs exhibit a linear correlation with the heat flux but a non-linear relationship with the electric current. By employing the CVF method and conformal mapping technique, the generalized analysis of a two-dimensional scenario involving an elliptic hole or crack in a TE material subjected to uniform ECD and EFL at infinity was conducted [6]. The findings indicated that the concentration factors of ECD and stress at the rim of the elliptic hole escalate as the major-to-minor axis ratio of the hole increases. The utilization of the CVF and Cauchy integrals enabled the resolution of the problem involving a circular in homogeneity embedded in TE materials exposed to uniform ECD and EFL [7]. The investigation revealed that the induced stress, resulting from both electrical and thermal effects, displayed a linear dependence on the energy flux applied at infinity. However, the relationship between the stress and the remote ECD was found to be nonlinear. An analytical model to assess fatigue cracking and its impact on the power of a hybrid photovoltaic TE device was proposed [8]. It was found that combining a TE module and a photovoltaic cell with a low temperature coefficient can increase total electric power.

The dimensionless SIFs are affected by crack length, crack spacing, and the bi-elastic constant ratio for dual collinear interface cracks on the electric potential and temperature of Thermoelectric Bonded Materials (TEBM) subjected to electric and thermal loads [9]. They solved SIFs using Laplace equations and the driving forces of ECD and EFL. The effect of fluid temperature and crack size toward stress intensity factor on geothermal pipe installations discussed the two key parameters which is fluid temperature and crack size. Specifically, the variations tested are fluid temperatures of 80°C, 115°C, and 150°C and crack sizes of 1 mm, 3 mm, and 5 mm. The material used for the geothermal pipe is ASTM A106-B steel, which is a standard material for such applications [10].

The investigation on numerical simulation of electromechanical impedance-based crack detection of heated metallic structures that investigate the influence of temperature on the detection of cracks using EMI. The results of the numerical simulations were compared to experimental impedance responses reported in the literature. These experiments involved the use of EMI to monitor various structures, both undamaged and damaged, constructed from steel and aluminium. The comparison showed that the Finite Element Models (FEM) developed in this study produced similar results with good agreement when compared to the experimental data. This suggests that numerical simulations using FEM could be a viable alternative to conducting physical experiments for studying the EMI approach in structural health monitoring [11]. Complex potential functions and Cauchy integrals were employed to address the challenge of analysing a circular inhomogeneity within thermoelectric materials under the influence of a uniform electric current

density and energy flux. The study uncovered that the stress induced by electrical and thermal factors exhibited a linear correlation with the energy flux imposed at an infinite distance, while displaying a nonlinear connection with the distant electric current density [12].

The finite element method, coupled with a collocation technique for enforcing kinematic constraints between strains and displacements, was employed to investigate issues related to nano-sized cracks in thermoelectric materials. The study aimed to assess the impact of size effects on the changes in crack opening displacements in relation to stress intensity factors (SIFs) at the tips of the cracks [13]. They effectively tackled a two-dimensional issue in their research, concentrating on the behavior of limitless thermoelectric materials. More specifically, they examined a scenario involving a circular aperture containing two unequal cracks. Their investigation encompassed the examination of how the system responded to both uniform electric current and thermal flux. Their findings indicated that the thermoelectric and stress intensity factors (SIFs) were influenced by factors such as the radius of the circular hole and the lengths of the cracks [14].

To the best of the authors' knowledge, there is a scarcity of information regarding the formulation of inclined crack problems in TEBM subjected to remote stress using Hypersingular Integral Equations (HSIEs). In this study, the problem is specifically addressed by formulating it into HSIEs through the utilization of the Modified Complex Variable Function (MCVF) method. The Continuity Conditions (CC) of the Resultant Electric Force (REF) and Displacement Electric Function (DEF) are taken into account, ensuring the smooth transition of temperature and resultant heat flux across the TEBM interface.

2. Methodology

2.1 Mathematical Formulation

The stresses, REF and DEF functions induced by the TE function can be obtained as follows [15]:

$$\sigma_x+\sigma_y=2\left[\phi'(z)+\overline{\psi'(z)}\right]+\frac{E\alpha\lambda}{\kappa}f(z)\overline{f(z)} \tag{1}$$

$$\sigma_y-\sigma_x+2i\sigma_{xy}=2\left[\bar{z}\phi''(z)\right]+\frac{E\alpha\lambda}{\kappa}f'(z)\overline{F(z)} \tag{2}$$

$$-Y+iX=\phi(z)+z\overline{\phi'(z)}+\overline{\psi(z)}+\frac{E\alpha\lambda}{\kappa}F(z)\overline{f(z)} \tag{3}$$

$$u+iv=\frac{1}{2G}\left[K\phi(z)-z\overline{\phi'(z)}-\overline{\psi(z)}\right]+\alpha\int\Omega(z)dz-\frac{E\alpha\lambda}{4G\kappa}F(z)\overline{f(z)} \tag{4}$$

where $\phi(z)$ and $\psi(z)$ are CVF, *G* is shear modulus, $K=(3-\mu)/(1+\mu)$, μ is Poisson's ratio, *E* is Young's modulus, α is the coefficient of thermal expansion, $\Omega(z)=-(\lambda/\kappa)f(z)^2+(2/\kappa)g(z)$, and $F(z)=\int f(z)dz$.

The derivative in a specified direction of REF (3) with respect to z yields the normal (*N*) and tangential (*T*) components of traction along the segment z, $z+dz$, where $dz/dz=-e^{-2i\theta}$ and θ is tangential angle to the crack as follows

$$\frac{d}{dz}\{-Y+iX\}=\phi'(z)+\overline{\phi'(z)}+\frac{d\bar{z}}{dz}\left(z\overline{\phi''(z)}+\overline{\psi'(z)}\right)+\frac{E\alpha\lambda}{4G\kappa}\left(f(z)\overline{f(z)}+F(z)\overline{f'(z)}\frac{d\bar{z}}{dz}\right)=N+iT \tag{5}$$

Note that the traction $N+iT$ depends on the position of point z and the direction of the segment $d\bar{z}/dz$.

The CVF, and unknown analytic function for electric and thermal fields for the case of an ICP in an infinite material can be expressed by [16-18]:

$$\phi(z)=\frac{1}{2\pi}\int_L\frac{g(t)dt}{t-z}$$

$$\psi(z)=\frac{1}{2\pi}\int_L\frac{g(t)}{t-z}+\frac{1}{2\pi}\int_L g(t)\left(\frac{d\bar{t}}{t-z}-\frac{\bar{t}dt}{(t-z)^2}\right)$$

$$f(z)=\frac{i\mathrm{J}}{2\lambda}\sqrt{z^2-a^2} \tag{6}$$

$$F(z)=\frac{i\mathrm{J}}{4\lambda}\left(z\sqrt{z^2-a^2}-a^2\ln\left(z+\sqrt{z^2-a^2}\right)\right)$$

$$g(z)=\frac{i\mathrm{U}}{2}\sqrt{z^2-a^2}$$

$$\Omega(z)=\frac{\mathrm{J}^2}{4\lambda\kappa}\left(z^2-a^2\right)+\frac{i\mathrm{U}}{\kappa}\sqrt{z^2-a^2}$$

where 2a is length of the crack and $g(t)$ is the COD function defined as

$$g(t)=\frac{2G}{i(K+1)}\left[\left(u(t)+iv(t)\right)^+-\left(u(t)+iv(t)\right)^-\right],(t\in L) \tag{7}$$

$\left(u(t)+iv(t)\right)^+$ and $\left(u(t)+iv(t)\right)^-$ denotes the displacement at a point *t* of the upper and lower crack faces, respectively.

Consider an ICP lies in both upper parts of TEBM subjected to remote stress as shown in Figure 1. The MCVF for an ICP lies in the upper parts of TEBM can be expressed by [15]:

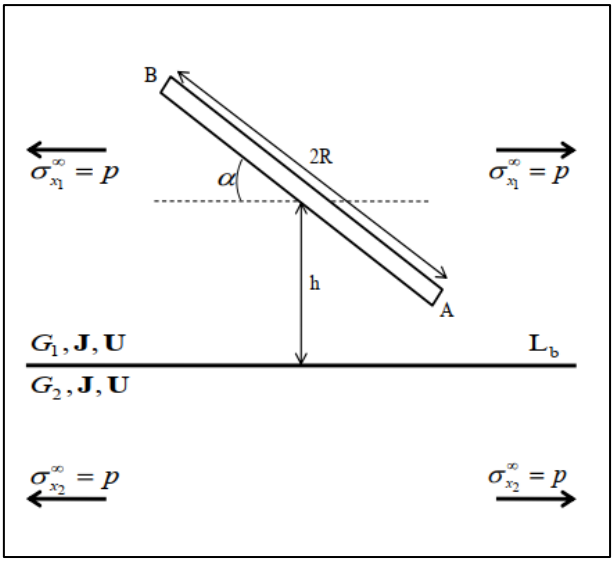

Fig. 1. An ICP lies in both upper parts of TEBM subjected to remote stress

$$\phi_1(z)=\phi_{1p}(z)+\phi_{1c}(z),\quad \psi_1(z)=\psi_{1p}(z)+\psi_{1c}(z) \tag{8}$$

where $\phi_{1p}(z)$ and $\psi_{1p}(z)$ are the principal part of the CVF and the elementary solution for isotropic medium (infinite materials), whereas $\phi_{1c}(z)$ and $\psi_{1c}(z)$ are the complementary part of the CVF. The CVF for a crack lies in the lower part of the TEBM are represented by $\phi_2(z)$ and $\psi_2(z)$. The CC of REF (3) by applying MCVF (8) yields

$$\begin{aligned}&\left[\phi_{1p}(t)+\phi_{1c}(t)+t\overline{\phi'_{1p}(t)}+\overline{\psi_{1p}(t)}+t\overline{\phi'_{1c}(t)}+\overline{\psi_{1c}(t)}+\frac{E_1\alpha_1\lambda_1}{4G_1\kappa_1}\left(F_{1p}(t)\overline{f_{1p}(t)}+F_{1c}(t)\overline{f_{1c}(t)}\right)\right]^{+}\\&\qquad=\left[\phi_2(t)+t\phi'_2(t)+\psi_2(t)\frac{E_2\alpha_2\lambda_2}{4G_2\kappa_2}F_2(t)\overline{f_2(t)}\right]\end{aligned} \tag{9}$$

whereas the CC of DEF (4) by applying MCVF (8) yields:

$$\begin{aligned}&G_2\left[K_1\phi_{1p}(t)+K_1\phi_{1c}(t)-\left(t\overline{\phi'_{1p}(t)}+\overline{\psi_{1p}(t)}\right)-\left(t\overline{\phi'_{1c}(t)}+\overline{\psi_{1c}(t)}\right)+2G_1\alpha_1\left(\int\Omega_{1p}(t)dt+\int\Omega_{1c}(t)dt\right)-\frac{E_1\alpha_1\lambda_1}{2\kappa_1}\left(F_{1p}(t)\overline{f_{1p}(t)}+F_{1c}(t)\overline{f_{1c}(t)}\right)\right]^{+}\\&\qquad=G_1\left[K_2\phi_2(t)-t\overline{\phi'_2(t)}-\overline{\psi_2(t)}+2G_2\alpha_2\int\Omega_2(t)dt-\frac{E_2\alpha_2\lambda_2}{2\kappa_2}F_2(t)\overline{f_2(t)}\right]^{-}\end{aligned} \tag{10}$$

Note that $t\in L_j$, $(j=1,2)$ along the crack interface, + and – sign represent the upper and lower parts of TEBM, respectively. By employing the method of analytical continuation, it becomes feasible to obtain the following expressions through the application of Eq. (9) and (10)

$$\phi_{1c}(z)=\Gamma_1\left(z\overline{\phi'_{1p}(z)}+\overline{\psi_{1p}(z)}\right)+\Gamma_2F_{1p}(z)f_{1p}(z)+\Gamma_3\int\overline{f_{1p}}^{2}(z)dz-\Gamma_4\int\overline{g_{1p}}(z)dz \tag{11}$$

$$\psi_{1c}(z)=\Gamma_5\overline{\phi_{1p}(z)}-z\phi'_{1c}(z)+\Gamma_6\overline{F_{1p}}(z)+\Gamma_7\int\overline{\Omega_{1p}}(z)dz+\Gamma_8\int\overline{f_{1p}}^2(z)dz-\Gamma_9\int\overline{g_{1p}}(z)dz \tag{12}$$

$$\begin{aligned}\phi_2(z)=&\Gamma_{10}\phi_{1p}(z)+\Gamma_{11}F_{1p}(z)\overline{f_{1p}}(z)+\Gamma_{12}F_{1p}(z)\overline{f_{1p}}(z)+\Gamma_7\int\Omega_{1p}(z)dz+\Gamma_8\int f^2{}_{1p}(z)dz\\&-\Gamma_9\int g_{1p}(z)dz\end{aligned} \tag{13}$$

$$\psi_2(z)=\Gamma_{13}\left(z\phi'_{1p}(z)+\psi_{1p}(z)\right)-z\phi'_2(z)+\Gamma_{14}F_{1p}(z)\overline{f_{1p}}(z)+\Gamma_{15}\int f^2{}_{1p}(z)dz+\Gamma_{16}\int g_{1p}(z)dz \tag{14}$$

where $\overline{\phi_{1p}}(z)=\overline{\phi_{1p}(\bar{z})}$, and Γ_j are bi-Elastic Constant Ratio (ECR) defined as

$$\Gamma_1=\frac{G_2-G_1}{G_1+G_2K_1},\quad \Gamma_2=\frac{(2G_2-1)E_1\alpha_1\lambda_1}{4\kappa_1(G_1+G_2K_1)}\left(\frac{\lambda_1-\lambda_2}{\lambda_1+\lambda_2}\right)^2,\quad \Gamma_3=\frac{2G_1G_2\alpha_1\lambda_1}{\kappa_1(G_1+G_2\kappa_1)}\left(\frac{\lambda_1-\lambda_2}{\lambda_1+\lambda_2}\right)^2,$$

$$\Gamma_4=\frac{4G_1G_2\alpha_1}{\kappa_1(G_1+G_2\kappa_1)}\left(\frac{\kappa_1-\kappa_2}{\kappa_1+\kappa_2}\right),\quad \Gamma_5=\frac{G_2K_1-G_1K_2}{G_1K_2+G_2},\quad \Gamma_6=\left(\frac{E_2\alpha_2\lambda_2(2G_1G_2+G_1K_2)}{4G_2\kappa_2(G_1K_2+G_2)}\right)\left(\frac{2\lambda_1}{\lambda_1+\lambda_2}\right)^2,$$

$$\Gamma_7=\frac{2G_1G_2\alpha_1}{(G_1K_2+G_2)},\quad \Gamma_8=\frac{2G_1G_2\alpha_2\lambda_2}{\kappa_2(G_1K_2+G_2)}\left(\frac{2\lambda_1}{\lambda_1+\lambda_2}\right)^2,\quad \Gamma_9=\frac{8G_1G_2\alpha_2\kappa_1}{\kappa_2(\kappa_1+\kappa_2)(G_1K_2+G_2)},$$

$$\Gamma_{10}=\frac{(K_1+1)G_2}{G_1K_2+G_2},\quad \Gamma_{11}=\frac{E_2\alpha_2\lambda_2(2G_1-1)}{4\kappa_2(G_1K_2+G_2)}\left(\frac{2\lambda_1}{\lambda_1+\lambda_2}\right)^2,\quad \Gamma_{12}=\frac{G_2E_1\alpha_1\lambda_1(1-2G_1)}{4G_1\kappa_1(G_1K_2+G_2)},$$

$$\Gamma_{13}=\frac{G_2(1+K_1)}{G_1+G_2K_1},\quad \Gamma_{14}=\frac{(K_1+2G_1)G_2E_1\alpha_1\lambda_1}{4G_1\kappa_1(G_1+G_2K_1)}\left(\frac{\lambda_1-\lambda_2}{\lambda_1+\lambda_2}\right)^2,\quad \Gamma_{15}=\frac{2G_1G_2\alpha_1\lambda_1}{\kappa_1(G_1+G_2K_1)}\left(\frac{\lambda_1-\lambda_2}{\lambda_1+\lambda_2}\right)^2$$

$$\Gamma_{16}=\frac{4G_1G_2\alpha_1}{\kappa_1(G_1+G_2K_1)}\left(\frac{\kappa_1-\kappa_2}{\kappa_1+\kappa_2}\right)$$

The HSIEs for an ICP lies in the upper part of TEBM can be obtained by substituting Eq. (11) and (12) into Eq. (5), and apply Eq. (6), then letting point *z* approaches t_0 on the crack and changing $d\bar{z}/dz$ into $d\bar{t}_0/dt_0$ yields

$$\left[N(t_0)+iT(t_0)\right]_1=\frac{1}{\pi}\int_L\frac{g(t)dt}{(t-t_0)^2}+\frac{1}{2\pi}\int_L M_1(t,t_0)g(t)dt+\frac{1}{2\pi}\int_L M_2(t,t_0)\overline{g(t)}dt+M_3(t,t_0)$$

where

$$M_2(t,t_0)=\frac{1}{(\bar{t}-\bar{t}_0)^2}\frac{d\bar{t}}{dt}+\left(\frac{1}{(\bar{t}-\bar{t}_0)^2}+\frac{2(t_0-t)}{(\bar{t}-\bar{t}_0)^3}\frac{d\bar{t}}{dt}\right)\frac{d\bar{t}_0}{dt_0}+\Gamma_1$$

$$\left[\frac{1}{(\bar{t}-t_0)^2}+\frac{1}{(t-\bar{t}_0)^2}+\left(\frac{1}{(\bar{t}-t_0)^2}+\frac{2(t_0-t)}{(\bar{t}-t_0)^3}\right)\frac{d\bar{t}}{dt}+\left(\frac{2(t_0-t_0)}{(t-\bar{t}_0)^3}-\frac{1}{(t-\bar{t}_0)^2}\right)\frac{d\bar{t}_0}{dt_0}\right]$$

$$M_2\left(t,t_0\right)=\frac{1}{\left(\bar{t}-\bar{t}_0\right)^2}\frac{d\bar{t}}{dt}+\left(\frac{1}{\left(\bar{t}-\bar{t}_0\right)^2}+\frac{2\left(t_0-t\right)}{\left(\bar{t}-\bar{t}_0\right)^3}\frac{d\bar{t}}{dt}\right)\frac{d\bar{t}_0}{dt_0}+$$

$$\Gamma_1\left[\frac{1}{\left(\bar{t}-t_0\right)^2}+\frac{1}{\left(t-\bar{t}_0\right)^2}+\left(\frac{1}{\left(\bar{t}-t_0\right)^2}+\frac{2\left(t_0-t\right)}{\left(\bar{t}-t_0\right)^3}\right)\frac{d\bar{t}}{dt}+\left(\frac{2\left(t_0-t_0\right)}{\left(t-\bar{t}_0\right)^3}-\frac{1}{\left(t-\bar{t}_0\right)^2}\right)\frac{d\bar{t}_0}{dt_0}\right]$$

$$M_3\left(t,t_0\right)=\Gamma_2\frac{\mathrm{J}^2}{4\lambda_1^2}\left(t_0^2-\alpha^2+\frac{t_0}{2\sqrt{t_0^2-\alpha^2}}\left(t_0\sqrt{t_0^2-\alpha^2}-\alpha^2\ln\left(t_0+\sqrt{t_0^2-\alpha^2}\right)\right)\right)+\left(\Gamma_2+\left(\Gamma_6-\Gamma_2\right)\frac{d\bar{t}_0}{dt_0}\right)\frac{\mathrm{J}^2}{4\lambda_1^2}$$

$$\left(\bar{t}_0^2-a^2+\frac{\bar{t}_0}{2\sqrt{\bar{t}_0^2-a^2}}\left(\bar{t}_0\sqrt{\bar{t}_0^2-a^2}-\alpha^2\ln\left(\bar{t}_0+\sqrt{\bar{t}_0^2-a^2}\right)\right)\right)+\Gamma_2\frac{\mathrm{J}^2}{4\lambda_1^2}\left(t_0-\bar{t}_0\right)$$

$$\left(3\bar{t}_0+\left(\bar{t}_0\sqrt{\bar{t}_0^2-a^2}-\alpha^2\ln\left(\bar{t}_0+\sqrt{\bar{t}_0^2-a^2}\right)\right)\frac{\bar{t}_0^2-\bar{t}_0-a^2}{2\left(\sqrt{\bar{t}_0^2-a^2}\right)^3}\right)\frac{d\bar{t}_0}{dt_0}+\Gamma_3\frac{\mathrm{J}^2}{4\lambda_1^2}\left(2\alpha^2-t_0^2-\bar{t}_0^2+\left(3\bar{t}_0^2-2t_0\bar{t}_0-\alpha^2\right)\frac{d\bar{t}_0}{dt_0}\right)$$

$$+\Gamma_4\frac{i\mathrm{U}}{2}\left(\sqrt{t_0^2-\alpha^2}-\sqrt{\bar{t}_0^2-\alpha^2}+\frac{2\bar{t}_0^2-\bar{t}_0t_0-\alpha^2}{\sqrt{\bar{t}_0^2-\alpha^2}}\frac{d\bar{t}_0}{d\bar{t}_0}\right)+\left[\left(\frac{\Gamma_7}{\kappa_1}-\frac{\Gamma_8}{\lambda_1}\right)\frac{\mathrm{J}^2}{4\lambda_1^2}\left(\bar{t}_0^2-\alpha^2\right)+\left(\frac{\Gamma_7}{\kappa_1}-\frac{\Gamma_9}{2}\right)i\mathrm{U}\sqrt{\bar{t}_0^2-\alpha^2}\right]$$

$$\frac{d\bar{t}_0}{d\bar{t}_0}+\left(\Gamma_{17}+\Gamma_{18}\right)\frac{\mathrm{J}^2}{4\lambda_1^2}\left[\sqrt{t_0^2-\alpha^2}\sqrt{\bar{t}_0^2-\alpha^2}+\left(t_0\sqrt{t_0^2-\alpha^2}-\alpha^2\ln\left(t_0+\sqrt{t_0^2-\alpha^2}\right)\right)\frac{\bar{t}_0}{2\sqrt{\bar{t}_0^2-\alpha^2}}\frac{d\bar{t}_0}{d\bar{t}_0}\right]$$

and

$$\Gamma_{17}=\frac{E_1\alpha_1\lambda_1}{4G_1\kappa_1},\qquad \Gamma_{18}=\frac{E_1\alpha_1\lambda_1}{4G_1\kappa_1}\left(\frac{\kappa_1-\kappa_2}{\kappa_1+\kappa_2}\right)^2$$

3. Results

3.1 Numerical results

The dimensional SIFs at crack tips *A* and *B* are defined as follows [19,20]

$$K_A=\left(K_1-iK_2\right)_A=\sqrt{2\pi}\lim_{s\to s_A}\sqrt{|s-s_A|}\left[\frac{-s_1H_1\left(s_1\right)}{\sqrt{a^2{}_1-s^2{}_1}}e^{-i\theta_A}\right]=\sqrt{\alpha_1\pi}F_A, \tag{16}$$

$$K_B=\left(K_1-iK_2\right)_B=\sqrt{2\pi}\lim_{s\to s_B}\sqrt{|s-s_B|}\left[\frac{-s_2H_2\left(s_2\right)}{\sqrt{a^2{}_2-s^2{}_2}}e^{-i\theta_A}\right]=\sqrt{\alpha_2\pi}F_B, \tag{17}$$

where

$$F_A = H_1\left(-a_1\right)e^{-i\theta_A} = F_{1A} + iF_{2A}, \quad F_B = H_2\left(-a_2\right)e^{-i\theta_B} = F_{1B} + iF_{2B}$$

Table 1 displays the dimensionless SIFs versus *h/R* at the crack tips *A* and *B* for an ICP in the upper part of TEBM for $a = 90^o$, and $\mathrm{J} = \mathrm{U} = 0$ as illustrated in Figure 2. Our findings align completely with those of Isida and Noguchi [18]. It is observed that the dimensionless SIFs at F_{2A} and F_{2B} are equals to zero. This phenomenon is due to the equivalence of the stress acting at the tips of the cracks. F_{1A} and F_{1B} are the Mode I dimensionless SIFs at crack tips *A* and *B*, respectively, and characterizes the amplitude of normal stress singularity. Whereas F_{2A} and F_{2B} are the Mode II dimensionless SIFs at crack tips *A* and *B*, respectively, and describes the amplitude of the shear stress singularity.

Table 1
Dimensionless SIFs versus *h/R* at the crack tips *A* and *B* for an ICP in the upper part of TEBM

G_2 / G_1	*h/R*					
	SIFs	1.2	1.4	1.6	1.8	2.0
0.25	$F_{1A}{}^a$	1.2213	1.1274	1.0857	1.0623	1.0476
	$F_{1A}{}^b$	1.2220	1.1280	1.0860	1.0630	1.0480
	$F_{1B}{}^a$	1.0783	1.0563	1.0432	1.0344	1.0281
	$F_{1B}{}^b$	1.0790	1.0570	1.0430	1.0350	1.0280
0.50	$F_{1A}{}^a$	1.1111	1.0653	1.0444	1.0324	1.0249
	$F_{1A}{}^b$	1.1120	1.0660	1.0450	1.0330	1.0250
	$F_{1B}{}^a$	1.0394	1.0289	1.0223	1.0179	1.0147
	$F_{1B}{}^b$	1.0400	1.0290	1.0220	1.0180	1.0150
2.00	$F_{1A}{}^a$	0.9032	0.9410	0.9592	0.9699	0.9767
	$F_{1A}{}^b$	0.9030	0.9410	0.9596	0.9700	0.9770
	$F_{1B}{}^a$	0.9656	0.9740	0.9795	0.9843	0.9863
	$F_{1B}{}^b$	0.9660	0.9740	0.9790	0.9830	0.9860
4.00	$F_{1A}{}^a$	0.8291	0.8944	0.9266	0.9455	0.9576
	$F_{1A}{}^b$	0.8290	0.8940	0.9270	0.9450	0.9580
	$F_{1B}{}^a$	0.9393	0.9535	0.9631	0.9701	0.9752
	$F_{1B}{}^b$	0.9390	0.9540	0.9630	0.9700	0.9750

^{a} Current study; ^{b} [18]

Figure 2 presents the dimensionless SIFs versus *h/R* at the crack tips *A* and *B* for an ICP in the upper part of TEBM for $a = 90^o$, $\mathrm{U} = 0$, and $\mathrm{J} = 20$. It is observed that the dimensionless SIFs for Mode I (F_{1A}) at crack tip A decreases as G_2 / G_1 increases, and as *h/R* increases F_{1A} decreases for G_2 / G_1 < 1.0 and increases for G_2 / G_1 > 1.0 as presented in Figure 2(a). whereas the dimensionless SIFs for Mode I (F_{1B}) at crack tip B increases as *h/R* increases for G_2 / G_1 > 1.0 and decreases for G_2 / G_1 < 1.0 as presented in Figure 2(b). This observation indicate that the strength of the materials become weaker as *h/R* increases for G_2 / G_1 > 1.0.

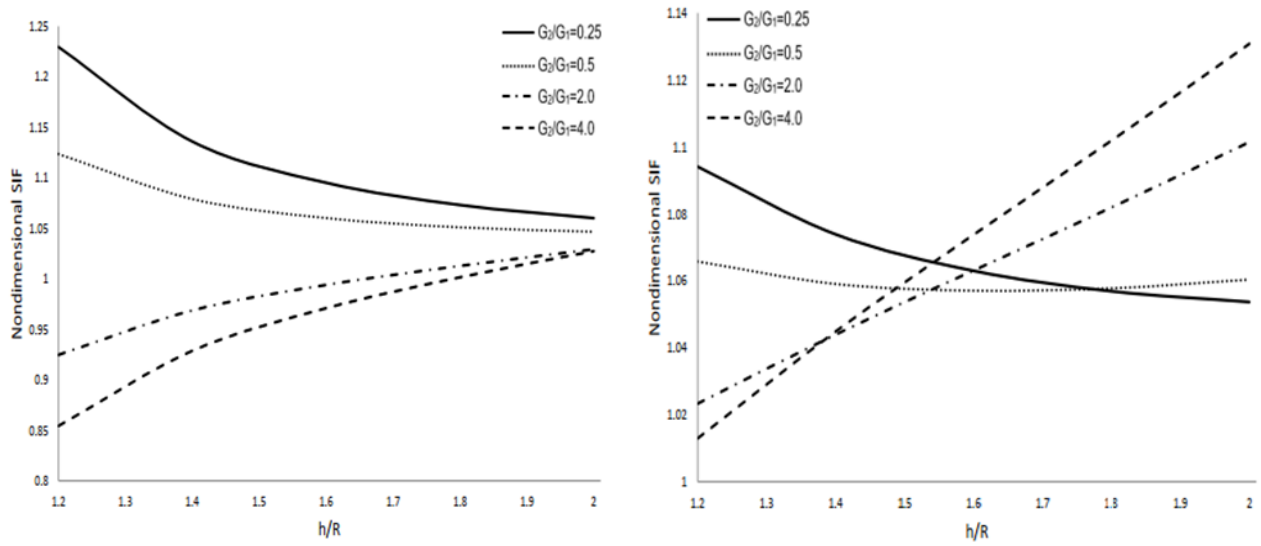

Fig. 2. Dimensionless SIFs F_{1A} (a) and F_{1B} (b) versus *h/R* at all crack tips for $a=90^o$, $\mathrm{U}=0$, and $\mathrm{J}=20$

Figure 3 presents the dimensionless SIFs for Mode I (Blue) and Mode II (Red) versus α at the crack tips *A* and *B* for an ICP in the upper part of TEBM for *h* = *R*/0.9, $\mathrm{U}=0$, and $\mathrm{J}=20$. It is observed that the dimensionless SIFs for Mode I (F_{1A} and F_{1B}, Blue) at all crack tips increases as α increases and decreases as G_2/G_1 increases as presented in Figure 3 (a). Whereas the dimensionless SIFs for Mode II (F_{2A} and F_{2B}, Red) at all crack tips decreases as G_2/G_1 increases and decreases as α increases for $a>50^o$. The observed trend indicates that an increase in α and a decrease in G_2/G_1 correspond to a weakening of the materials' strength.

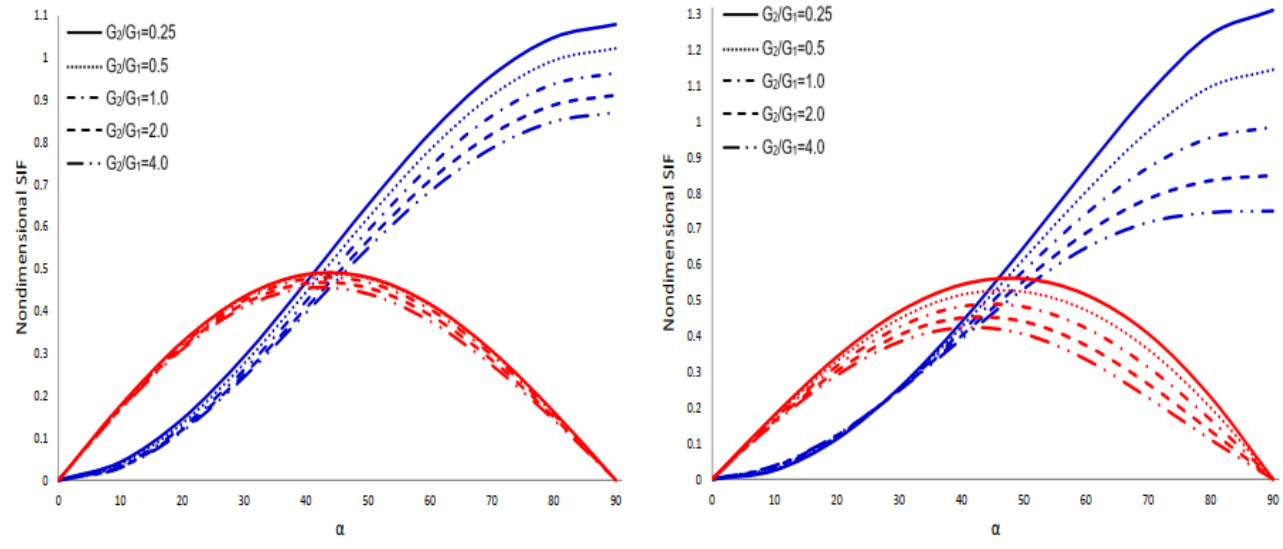

Fig. 3. Dimensionless SIFs F_{1A} (a) and F_{1B} (b) versus *h/R* at all crack tips for *h* = *R*/0.9, $\mathrm{U}=0$, and $\mathrm{J}=20$

4. Conclusions

In this particular investigation, we have focused on tackling an ICP occurring in the upper part of TEBM under the presence of remote stress. Although the problem itself has historical origins, our study introduces several distinctive elements. Primarily, the application of the MCVF in this work represents a novel approach for addressing crack problems specifically in TE materials. Through this innovative methodology, HSIEs are derived, with the COD function, ECD, and EFL between the crack tips being considered as the key unknown variables. The general solution of HSIEs for an ICP lies in the upper part of TEBM have been obtained. The analysis of numerical results leads to the conclusion that the dimensionless SIFs for an ICP situated in the upper part of TEBM are dependent on several factors. These factors encompass the ECR, ECD, crack geometries, as well as the distance between the crack and the boundary. This condition will be effected on the strength of the materials. On the basis of this study, we believe that several extensions are possible, such as cohesive models, cracks at the interface bonded materials, cracks issued by inclusions, three-dimensional cracks problems in TEBM, and so on. Based on the current study, a detailed formulation with numerical analysis will be published elsewhere. More research is being conducted to broaden the application field of the developed concept.

Acknowledgement

We express our gratitude for the financial support received from the Ministry of Higher Education (Malaysia) through the grants: FRGS/1/2021/STG06/UTEM/03/2 and Universiti Teknikal Malaysia Melaka. Additionally, we extend our appreciation for the research assistance provided by Universiti Putra Malaysia.

References

[1] Wang, P., B. L. Wang, and K. F. Wang. "Dynamic response of cracked thermoelectric materials." *International Journal of Mechanical Sciences* 160 (2019): 298-306. https://doi.org/10.1016/j.ijmecsci.2019.06.047

[2] Jiang, Dongdong, Qing-Hui Luo, Wei Liu, and Yue-Ting Zhou. "Thermoelectric field disturbed by two unequal cracks adjacent to a hole in thermoelectric materials." *Engineering Fracture Mechanics* 235 (2020): 107163. https://doi.org/10.1016/j.engfracmech.2020.107163

[3] Song, Hao-Peng, Cun-Fa Gao, and Jiangyu Li. "Two-dimensional problem of a crack in thermoelectric materials." *Journal of Thermal Stresses* 38, no. 3 (2015): 325-337. https://doi.org/10.1080/01495739.2015.1015369

[4] Ngaongam, Choosak, and Rapee Ujjin. "FEM Modelling of the Heating Behaviour in Vibrothermography Based on Thermoelastic Damping on Crack Location." *Journal of Advanced Research in Fluid Mechanics and Thermal Sciences* 108, no. 1 (2023): 66-74. https://doi.org/10.37934/arfmts.108.1.6674

[5] Cheok, Choon Yoong, and Anusuyah Ragunathan. "Anthocyanin degradation kinetics and thermodynamic analysis of Hibiscus rosa-sinensis L. Clitoria ternatea L. and Hibiscus sabdariffa L." *Progress in Energy and Environment* (2022): 1-12. https://doi.org/10.37934/progee.19.1.112

[6] Zhang, A. B., and B. L. Wang. "Explicit solutions of an elliptic hole or a crack problem in thermoelectric materials." *Engineering Fracture Mechanics* 151 (2016): 11-21. https://doi.org/10.1016/j.engfracmech.2015.11.013

[7] Yu, Chuan-Bin, Hai-Bing Yang, Yu-Hao Li, Kun Song, and Cun-Fa Gao. "Closed-form solutions for a circular inhomogeneity in nonlinearly coupled thermoelectric materials." *ZAMM-Journal of Applied Mathematics and Mechanics/Zeitschrift für Angewandte Mathematik und Mechanik* 99, no. 8 (2019): e201800240. https://doi.org/10.1002/zamm.201800240

[8] Cui, Y. J., B. L. Wang, K. F. Wang, G. G. Wang, and A. B. Zhang. "An analytical model to evaluate the fatigue crack effects on the hybrid photovoltaic-thermoelectric device." *Renewable Energy* 182 (2022): 923-933. https://doi.org/10.1016/j.renene.2021.10.076

[9] Jiang, Dongdong, and Yue-Ting Zhou. "Role of crack length, crack spacing and layer thickness ratio in the electric potential and temperature of thermoelectric bi-materials systems." *Engineering Fracture Mechanics* 259 (2022): 108170. https://doi.org/10.1016/j.renene.2021.10.076

[10] Anam, Khairul, Anindito Purnowidodo, and Hastono Wijaya. "The Effect of Fluid Temperature and Crack Size toward Stress Intensity Factor on Geothermal Pipe Installations." *Journal of Advanced Research in Fluid Mechanics and Thermal Sciences* 54, no. 1 (2019): 27-36.
[11] Djemana, Mohamed, Meftah Hrairi, and Norfazrina Hayati Mohd Yatim. "Numerical Simulation of Electromechanical Impedance Based Crack Detection of Heated Metallic Structures." *Journal of Advanced Research in Fluid Mechanics and Thermal Sciences* 94, no. 2 (2022): 77-88. https://doi.org/10.37934/arfmts.94.2.7788
[12] Yu, Chuan-Bin, Hai-Bing Yang, Yu-Hao Li, Kun Song, and Cun-Fa Gao. "Closed-form solutions for a circular inhomogeneity in nonlinearly coupled thermoelectric materials." *ZAMM-Journal of Applied Mathematics and Mechanics/Zeitschrift für Angewandte Mathematik und Mechanik* 99, no. 8 (2019): e201800240. https://doi.org/10.1002/zamm.201800240
[13] Sladek, Jan, Vladimir Sladek, Miroslav Repka, and Siegfried Schmauder. "Crack analysis of nano-sized thermoelectric material structures." *Engineering Fracture Mechanics* 234 (2020): 107078. https://doi.org/10.1016/j.engfracmech.2020.107078
[14] Jiang, Dongdong, Qing-Hui Luo, Wei Liu, and Yue-Ting Zhou. "Thermoelectric field disturbed by two unequal cracks adjacent to a hole in thermoelectric materials." *Engineering Fracture Mechanics* 235 (2020): 107163. https://doi.org/10.1016/j.engfracmech.2020.107163
[15] Song, K., H. P. Song, P. Schiavone, and C. F. Gao. "Electric current induced thermal stress around a bi-material interface crack." *Engineering Fracture Mechanics* 208 (2019): 1-12. https://doi.org/10.1016/j.engfracmech.2019.01.004
[16] Long, NMA Nik, and Z. K. Eshkuvatov. "Hypersingular integral equation for multiple curved cracks problem in plane elasticity." *International Journal of Solids and Structures* 46, no. 13 (2009): 2611-2617. https://doi.org/10.1016/j.ijsolstr.2009.02.008
[17] Chen, Y. Z., and N. Hasebe. "Stress-intensity factors for curved circular crack in bonded dissimilar materials." *Theoretical and applied fracture mechanics* 17, no. 3 (1992): 189-196. https://doi.org/10.1016/0167-8442(92)90027-U
[18] Isida, M., and H. Noguchi. "Arbitrary array of cracks in bonded half planes subjected to various loadings." *Engineering fracture mechanics* 46, no. 3 (1993): 365-380. https://doi.org/10.1016/0013-7944(93)90230-P
[19] Hamzah, Khairum Bin, Nik Mohd Asri Nik Long, Norazak Senu, and Zainidin K. Eshkuvatov. "Numerical solution for crack phenomenon in dissimilar materials under various mechanical loadings." *Symmetry* 13, no. 2 (2021): 235. https://doi.org/10.3390/sym13020235
[20] Mohd Nordin, Muhammad Haziq Iqmal, Khairum Bin Hamzah, Najiyah Safwa Khashi'ie, Iskandar Waini, Nik Mohd Asri Nik Long, and Saadatul Fitri. "Formulation for Multiple Cracks Problem in Thermoelectric-Bonded Materials Using Hypersingular Integral Equations." *Mathematics* 11, no. 14 (2023): 3248. https://doi.org/10.3390/math11143248